

Estimation of Regional Evapotranspiration based on Tri-Angle Method Using Thermal and VNIR Data.

Abstract

Evapotranspiration is a critical component in the hydrological cycle, water resources management and climate studies especially in arid and semi-arid regions. This paper aimed at producing a simplified and applicable procedure for estimating spatial distributed daily actual evapotranspiration (ET_a) directly at regional scale using thermal and visible-near infra-red (VNIR) data. Triangle method, which makes a parameterization of Priestly-Taylor equation, was used to estimate ET_a at daily scale directly by using a simplified approach with realistic hypotheses. This study conducted in Egypt, Salhia, 6th of October Company as an arid region over the winter crops (wheat, potato and sugar beet) cultivated there using multi date Landsat images. The results were compared with ET_a values adjusted from crop evapotranspiration ET_c “FAO Penman-Monteith approach” using the Crop Water Stress Index (CWSI). The results showed high accuracy and good agreement against assessment method. The correlation factor (R^2) values for wheat, potato and sugar beet were 0.88, 0.98 and 0.99 and Root Mean Square Error (RMSE) were 0.2, 0.26 and 0.37 respectively over the different dates. In the 16th of April, 2014 there was a significant difference in wheat curves as the RMSE were 0.8 and we explained the reasons of this difference as it is a result of the sprinkler irrigation system effect on the mature wheat. This results show that the proposed procedure is accurate enough at least in most cases of our study for estimating the regional surface ET_a but it need to evaluate for wheat under other irrigation systems like surface or drip irrigation systems .

Keywords: Remote sensing, ET_a , Landsat, CWSI and Arid regions.

1. Introduction

Fresh water resources are becoming increasingly limited in many parts of the world, and decision makers are demanding new tools for monitoring water availability and rates of consumption [26]. The water shortage is the main constraint and a major limiting factor facing the implementation of the country’s future economic development plans [27]. Global estimates of water consumption by sector indicate that irrigated agriculture is responsible for 85% of the water-use and that consumption in this sector will increase by 20% by 2025 [10]. In general, water availability is a major limitation for crop production and agriculture development specially, in arid and semi-arid regions. Egypt is under the water poverty line, as the per capita is less than 650 m³/year. In addition to water poverty, Egypt faces a great danger due to the millennium dam in Ethiopian, which will lead to water quota shortage from the Nile River. As the agriculture sector is the largest consumer of fresh water, so it will be the first and largest sector influenced by this shortage. Management water resources, developing irrigation systems and actual water requirements studies must be conduct in order to face this danger. A better understanding of the water balance is essential for exploring water saving techniques. One of the most important concepts regarding water balance in arid and semi-arid areas is crop evapotranspiration (ET_c) which is a key factor for determining proper irrigation scheduling and for improving water use

43 efficiency in irrigated agriculture [11-41]. Large volumes of water transfer from the soil and
44 vegetation to atmosphere by evapotranspiration (*ET*). Accurate, spatially distributed information
45 on water use, quantified at the scale of human influence, has been a long-standing critical need
46 for a wide range of applications. Quantifying *ET* for irrigated crops in arid regions is vital to
47 water resources management. The detailed *ET* maps enable managers to allocate available water
48 precisely among agricultural, urban, and environmental uses. The actual rate of water use by
49 vegetation can deviate significantly from potential *ET* rates due to impacts of drought, disease,
50 insects, vegetation amount, phenology, soil texture, fertility and salinity [1-2-26]. Different
51 methods have been proposed for measuring *ET* on various spatial scales from individual plants to
52 fields or landscape scales. However, conventional techniques provide essentially point
53 measurements, which usually do not represent areal means because of the heterogeneity of land
54 surfaces and the dynamic nature of heat transfer processes [39-40]. In recent years, as a result of
55 the enormous developments in remote sensing technology, satellite data specifications, spatial,
56 temporal and spectral resolution, are continuously improving. Many surface parameters, such as
57 albedo, vegetation coverage, land surface temperature, and leaf area index, can be retrieved from
58 visible, near-infrared, thermal infrared and other bands of satellite data. These data provide a
59 basis for estimating *ET* from farmland and other regions and have attracted widespread attention
60 for the use of remote sensing technologies to study regional *ET* [25]. Over the last few decades,
61 different physical and empirical remote sensing based models, which vary in complexity,
62 accuracy, and needing for ancillary metrological data, have been proposed for estimating *ET* at
63 different scales. In general, Accuracy in estimating *ET* basically depend on the accuracy of the
64 input satellite data products, such as land surface temperature (*LST*), normalized difference
65 vegetation index (*NDVI*), surface emissivity (ϵ_s) and surface albedo (α). However, the satellite
66 derived variables are in turn and it depend on factors relating to residual atmospheric effects,
67 spatial and temporal resolution, viewing angles, etc. Ancillary surface and atmospheric data like
68 wind speed, aerodynamic resistance, and surface roughness, which cannot readily be measured
69 through remote sensing techniques, usually required for these models. Therefore, it is still
70 challenging to estimate and produce *ET* maps at regional and even global scale using satellite
71 remote sensing without ground measurements or reanalyzed meteorological data. In order to
72 overcome this problem, some attempts have been made to develop new parameterizations for *ET*
73 estimation that depend entirely on remote sensing [30]. One widely used approach among them
74 is the *LST-NDVI* triangle method, which was proposed by [19-20] and improved by [21]. Briefly,
75 this method shows the relationship and the incident interaction between the soil, vegetation and
76 weather conditions. The *NDVI* values refer to the land cover type while, *LST* is a function in
77 weather conditions and soil moisture content. This method is based on the *P-T* (Priestley–
78 Taylor) equation [32], which can be considered as a simplified version of the more general
79 Penman equation [31]. The most sensitive point in this approach is the determination of ϕ which
80 substituted for the *P-T* parameter and accounts for aerodynamic and canopy resistances and
81 ranges from 0 at no *ET* to 1.26 at maximum *ET*. The ϕ parameter is estimated from the triangular
82 shape of the *LST-NDVI* feature space, which is formed by the scatterplot of *LST* versus *NDVI*
83 over a wide range of soil moisture content and fractional vegetation cover. The formalization of
84 the triangular shape is caused primarily by different sensitivity of *LST* to soil moisture variations
85 over bare soil and vegetated areas. There are several studies replaced the *NDVI* with other
86 Vegetation Indices (*VI*) such as fractional vegetation cover (*Fr*) [24-38] or broadband surface
87 albedo [41]. The advantages of *LST-VI* triangle method versus the other methods of surface
88 energy balance for estimating *ET* are that:- 1) very high accuracy in *LST* retrieval and

89 atmospheric correction are not indispensable, 2) needless to parameterize the complex
90 aerodynamic resistance and uncertainty originated from replacement of aerodynamic temperature
91 with LST is by passed, 3) it depends completely on remotely sensed LST and VI , 4) a direct
92 calculation of evaporative fraction (EF), and 5) estimations of the Evaporative Fraction (EF) and
93 the Net Radiation (Rn) are independent from each other. Therefore, the overall errors in ET can
94 be traced back to EF and Rn separately. There are some other methods making the estimation of
95 EF and Rn dependent on each other [3-29], thus making it impossible to trace errors separately.
96 Limitations of $LST-VI$ triangle mainly lie in a bit subjective determination of both dry and wet
97 edges and a large number of pixels required over a flat area with a wide range of soil moisture
98 and fractional vegetation cover [38]. The triangle method has been applied successfully in certain
99 applications for estimation of both ET [13-20-28-33-34-35] and soil moisture [7-37]. The main
100 objective of this study is estimating daily ET_a directly with no need to estimate the net radiation
101 (Rn) and evaporative fraction (EF) instantaneously by using a simplified approach during the
102 winter agriculture season in the different growth stages of the crops cultivated in the study area.

103

104 **2. Materials and Methods**

105 **2.1 Study area description**

106 El-Salhia project is located at the eastern part from Nile Delta as shown in (Fig. 1) and its
107 climate is dry arid according to Köppen Climate Classification System. The whole area of the
108 project is about 13,800 ha. Two irrigation systems are used in the project; the sprinkler irrigation
109 center pivot and the drip irrigation. The project has about 100 center pivot irrigation units. Each
110 pivot unit irrigates an area of about 63.6 ha. The common pivots length in the project is about
111 450 meter.

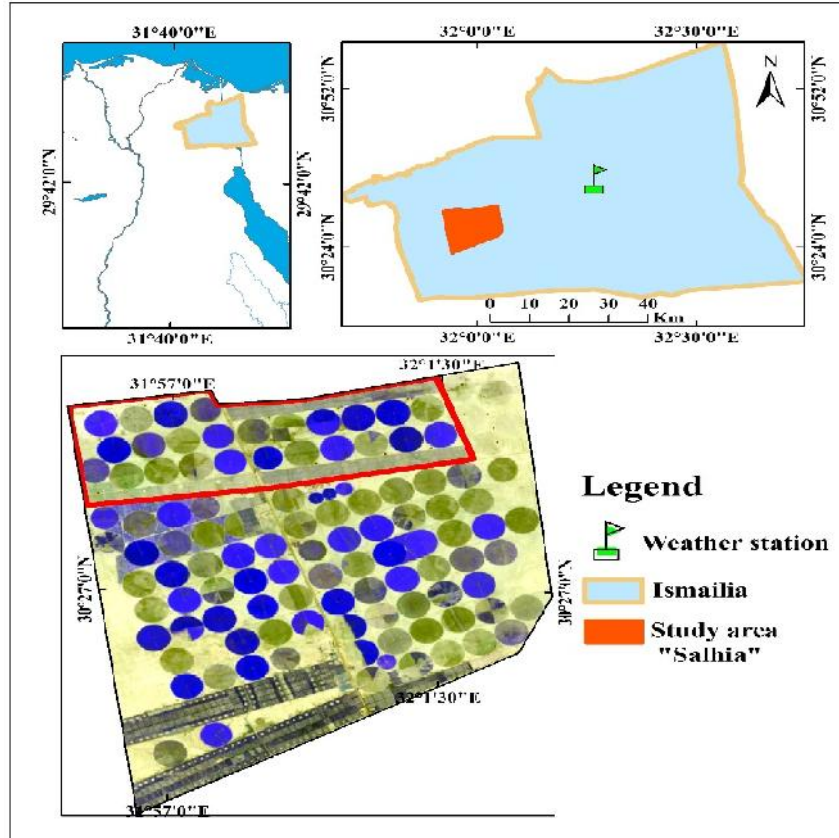


(Figure 1) Location map of the study area “ Salhia”.

2.2 Data availability

Satellite data: a combination of Landsat 7 and Landsat 8 (Path = 176 and Row = 39) were used to cover winter season crops. Table (1) illustrates the details of Landsat 7 and 8 satellite data.

Table (1) illustrates the Landsat 7 and 8 satellite data details.

No.	Date	Sensor type	Spatial resolution	Number of bands
1	17-12-2013	Landsat 7	30m×30m	8
2	02-01-2014	Landsat 7		8
3	11-02-2014	Landsat 8		11
4	15-03-2014	Landsat 8		11
5	31-03-2014	Landsat 8		11
6	16-04-2014	Landsat 8		11
7	02-05-2014	Landsat 8		11

Climatic metrological data: ground meteorological data namely air temperature, wind speed, dew point temperature and net radiation was used in order to calculate reference evapotranspiration (ET_0) during the days of the study.

2.3 ET_a estimation

The method applied here aimed to estimate daily ET_a directly by using the daily component of the energy balance equation eq.1;

125
$$R_n = G + H + \lambda E \quad (1)$$

126 Where; R_n is net radiation (Wm^{-2}), G is the soil heat flux (Wm^{-2}), H is the sensible heat flux
 127 (Wm^{-2}) and λE is the latent heat flux that is associated with the actual ET (Wm^{-2}). The energy
 128 balance can be rewritten to;

129
 130
$$\lambda E = EF \cdot (R_n - G) \quad (2)$$

131 Where; EF is the dimensionless evaporative fraction and $(R_n - G)$ equals the net available
 132 energy for ET . G can often be ignored for time scales of 1 day or more, and thus λE is a function
 133 of R_n and EF only [42]. The EF is also defined as the ratio of actual ET to the available energy
 134 (dimensionless).

135
$$EF = \frac{\lambda E}{R_n - G} \quad (3)$$

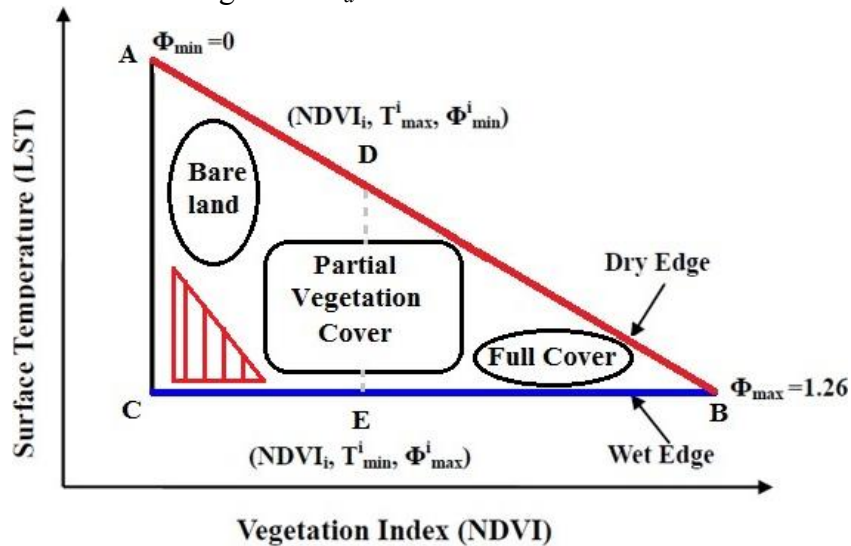
136 The common formula which represents the Triangle method (Priestley and Taylor, 1972) was
 137 used in this study according to (Priestley–Taylor) equation;

138
$$\lambda E = \phi[(R_n - G) \frac{\Delta}{\Delta + \gamma}] \quad (4)$$

139 Where; ϕ is a substituted for $P-T$ parameter, Δ is the slope of saturated vapor pressure at the air
 140 temperature (kPa/K) and γ is the psychrometric constant (kPa/K) and from eq. 2, 3 and 4, EF can
 141 be rewritten as;

142
$$EF = \frac{\lambda E}{R_n - G} = \phi \left(\frac{\Delta}{\Delta + \gamma} \right) \quad (5)$$

143 $LST-NDVI$ triangle method (Fig. 2) was applied in this study in order to estimate ϕ parameter. It is
 144 originated from the parameterization of [19], in a simplified $P-T$ formula [32]. Regional ET_a and
 145 EF were estimated according to Eq. (4) which depends almost completely on remotely sensed
 146 data. The accurate interpreting of the scatter plot which resulted from remotely sensed LST and
 147 $NDVI$ under conditions of variance ranges of soil moisture availability and vegetation cover
 148 leads to accurate estimation of regional ET_a .



149
 150 (Fig.2) Schematic diagram interpret the scatter plot of $(LST-NDVI)$ triangular space to estimate
 151 evaporative fraction using wet and dry surfaces assumption and data distribution entire the triangle.

152
 153 The dry edge is the oblique red solid line (*AB*) and the wet edge is the horizontal blue solid line
 154 (*CB*) represent the minimum *ET* and maximum *ET*, respectively. The two boundaries (dry and
 155 wet edges) of the *LST-NDVI* feature space represent limiting conditions for the surface fluxes.
 156 These edges respectively represent two limiting cases of soil moisture content and so evaporative
 157 fraction for each *NDVI* value (i.e., the unavailability of soil moisture and stressed vegetation at
 158 the dry edge and non-stressed vegetation which evaporate potential *ET* at the wet edge).
 159 Specifically, *EF* at the wet edge is EF_{max} ($EF_{max}=1$) so, pixels at the wet edge are regarded to
 160 evaporate/transpire potentially while at the dry edge, *EF* varies from EF_{min} ($EF_{min}=0$) at the dry
 161 bare soil to EF_{max} ($EF_{max}=1$) at fully non stressed vegetation cover when availability of root zone
 162 soil water is good. At the dry edge, ET_a mainly comes from the transpiration of vegetation from
 163 the root zone water as the soil surface hasn't enough water to evaporate. The values of (ϕ) also
 164 ranges from ($\phi_{min} = 0$) at dry bare soil pixels to ($\phi_{max} = 1.26$) at non stressed with full vegetation
 165 cover pixels and the other ϕ values for each pixel are based on its soil water content and partial
 166 vegetation cover. In the absence of significant advection and convection, ϕ in eq. (4 and 5) can
 167 take a wider range of 0 (no *ET*) to $\left(\frac{\Delta+Y}{\Delta}\right)$ (maximum *ET*).

168 Determination of dry and wet edges in the *LST-NDVI* scatter is necessary, to estimate pixel by
 169 pixel *ET* and *EF* using Eqs. (4) and (5). In arid and semi-arid areas, it should be noted that, for
 170 given vegetation cover, spatial pixels with high surface temperature and low *EF* are detectable
 171 by satellite remote sensors. On the other hand, the saturated soil water which evaporates
 172 potentially pixels is rarely and hardly existed in these conditions (see red lined triangle inside
 173 fig.2).

174 Obtaining of the ϕ value for each pixel requires a three step linear interpolation scheme based on
 175 the *LST-NDVI* triangle which used to allocate ϕ values inside the scatterplot (Fig. 2); (1)
 176 determines the dry and wet edges in the triangular space. The *EF* estimation accuracy depends
 177 basically on the accuracy of determining wet and dry edges; (2) minimum and maximum ϕ are
 178 respectively set to $\phi_{min} = 0$ for the driest bare soil pixel “with lowest *NDVI* and highest *LST*”
 179 (point A) and $\phi_{max} = 1.26$ for the full vegetated pixel “with largest *NDVI* and lowest *LST*”
 180 (point B). For each $NDVI_i$ value, there are max and min values of ϕ_i , $\phi_{i_{max}}$ located on the wet
 181 edge (point E) ($\phi_{i_{max}}$ is generally set to $\phi_{i_{max}} = \phi_{max} = 1.26$) and $\phi_{i_{min}}$ Located on the dry edge
 182 (point D). 3) Finally, ϕ_i entire each *NDVI* value, is linearly interpolated between $\phi_{i_{min}}$ and $\phi_{i_{max}}$
 183 through the similarity between the *ABC* and *EBD* triangles (Fig. 2). The following relation is
 184 taking out from the similarity;

$$\frac{AD}{AB} = \frac{ED}{AC}$$

185 Thus, by converting the symbols into real parameters, ϕ value for each pixel can be calculated
 186 using the given mathematical expression as follows;

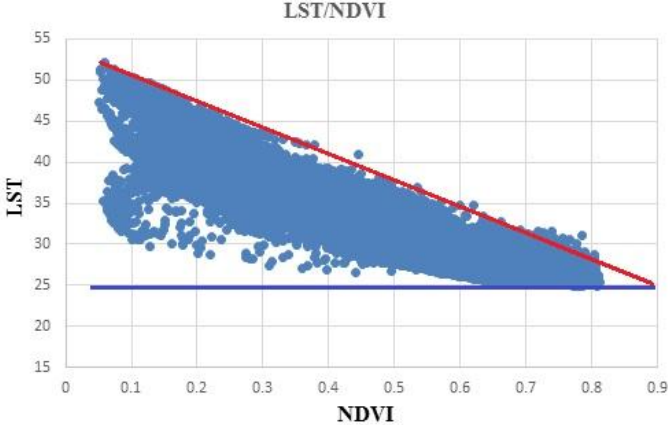
$$\phi_i = \left[\left(\frac{T_{max} - T_i}{T_{max} - T_{min}} \right) * (\phi_{max} - \phi_{min}) \right] + \phi_{min} \quad (6)$$

189
 190 Since the ϕ_{min} is equal to zero and ϕ_{max} is equal to 1.26, the eq.6 becomes as:

$$\phi_i = \left(\frac{T_{max} - T_i}{T_{max} - T_{min}} \right) * 1.26 \quad (7)$$

193

194 The above scheme accuracy depend on the accurate determination of the dry and wet edges, as
 195 the eq.7 depends on T_{max} which represents the high value on the dry edge and T_{min} which
 196 represents the wet edge as optimal conditions for ET . Also, intensive care during the pre-
 197 processing and extracting the LST from the remote sensing data must be taken into account.
 198 (Fig.3) represents of the relation between LST and $NDVI$ for sample of our data which illustrates
 199 the triangle shape and both of dry edge (oblique red line) and wet edge (horizontal blue line).



200
 201 (Fig.3) Scatterplot which illustrates the triangle shape and both of dry edge (oblique red line) and
 202 wet edge (horizontal blue line).

203
 204 Daily (24 hours) R_n according was estimated by using the [3] equation as [1] and [9] used the
 205 following equation to calculate it;

$$R_{n24} = (1-\alpha)R_{s\downarrow} - 110\tau_{sw24} \quad (8)$$

207 Where; R_{n24} is the daily net radiation (wm^{-2}), α is the surface albedo, $R_{s\downarrow}$ is the 24hour solar
 208 radiation (wm^{-2}) and τ_{sw24} is the atmospheric transmissivity.

209 The following assumption was used to estimate daily ET values in a direct way; the near noon
 210 instantaneous EF , which estimated by the triangle method was used as a representative value to
 211 the daily average EF value based on the observations of [6-8] for both homogeneous and
 212 heterogeneous land surfaces EF remains fairly constant for daylight hours, particularly at about
 213 10:00 and 16:00 O'clock and this assumption used by [30]. During daytime, EF is mainly
 214 controlled and determined by land surface properties such as vegetation amount, soil moisture
 215 and surface resistance to heat and momentum transfer. Most of them are slowly varying
 216 parameters during daytime as compared to other fast changing variables (e.g., surface
 217 temperature and radiation), which have much stronger diurnal cycles due to radiation and
 218 atmospheric forcing [22]. On the other hand, analysis of our hourly climate data showed that the
 219 difference between meteorological parameters such as air temperatures and relative humidity at
 220 the satellite overpass time and the daily average of these parameters were not considerable. The
 221 highest relative error value of air temperature and relative humidity values during the overpass
 222 time value and the average daily value was not exceed 9.8% and 15% respectively over the seven
 223 used dates of data. Hence, we can regard the weather conditions during the satellite overpass
 224 time are representative of the whole day and EF too. In addition to, several studies have
 225 concluded that using local near noon EF instead of daily EF for daily ET estimation incurs very
 226 small error [14-15-16-18].

227
228

$$ET_{\text{daily}} = (R_{n \text{ daily}} - G_{\text{daily}}) * EF_{\text{daily}} \quad (9)$$

229 As the daily G ignored in this study, as it is usually assumed negligible over the diurnal cycle or
230 day time scale [12-22-36-38]. The above equation can be rewritten as;

231
232

$$ET_{\text{daily}} = (R_{n \text{ daily}} * EF_{\text{daily}}). \quad (10)$$

233 2.4 Validation strategy.

234 Crop Evapotranspiration (ET_c) has been used to check the performance and the results of the
235 proposed procedure by converting it from ET_c to actual ET_a using the crop water stress index
236 ($CWSI$) extracted from satellite images. ET_c calculated by multiplying FAO table crop
237 coefficient (K_c) and reference evapotranspiration ET_o . There are many different approaches used
238 for estimating reference ET_o such as Penman-Monteith, Blaney-Criddle and Hargreaves
239 Samani [30-31]. Here, we used the FAO-Penman-Monteith (FPM) equation to calculate the
240 ET_o . The $CWSI$ is based on observed canopy-air temperature differences and is an index for the
241 water availability in the soil. When a crop with full cover has adequate water it will transpire at
242 the potential rate for that crop. The actual evapotranspiration ET_a rate will fall below the
243 potential rate when water becomes limiting [4-5-17-23]. The $CWSI$ ranges from 0 (no stress) to 1
244 (maximum stress) and has been defined as:

$$245 \quad CWSI = 1 - (ET_a / ET_c) \quad (11)$$

246 The following expression used to calculate $CWSI$ as a function in difference in LST .

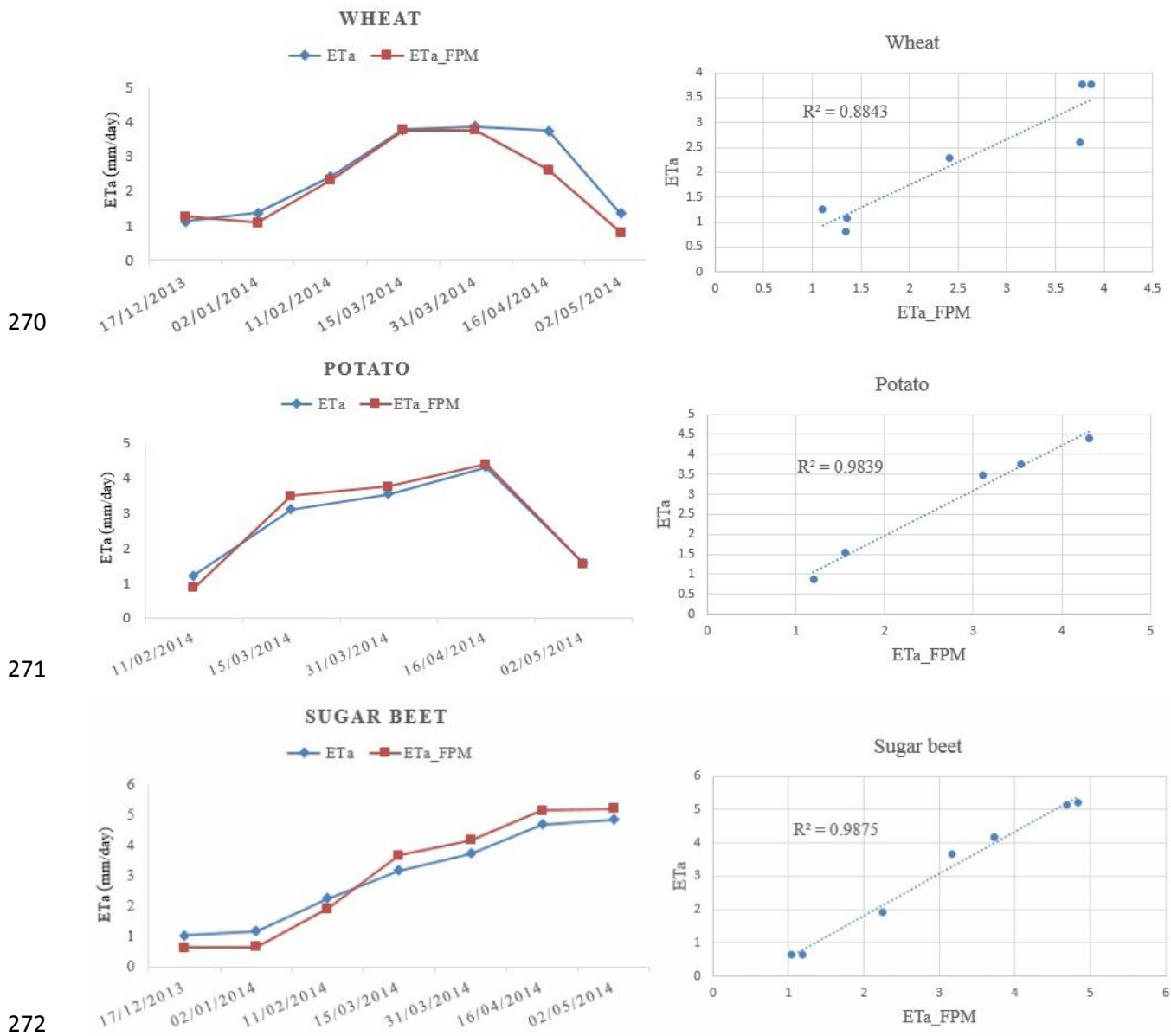
$$247 \quad CWSI = \frac{(T_i - T_{min})}{(T_{max} - T_{min})} \quad (12)$$

248 Where; T_i is the LST of each pixel, T_{min} is the minimum LST , T_{max} is the maximum LST at the
249 study area. This strategy was applied to verify the accuracy of the results of this approach on the
250 wheat, potato and sugar beet crops during the different growth stages.

251 3. Results and Discussions

252 Daily ET_a was calculated by using eq.10, which consist of two main components EF and R_n . EF
253 estimated by triangle method, which parameterize ($P-T$) parameter from the $LST/NDVI$ scatter
254 plot. The parameter (ϕ) is a down samples coefficient for both aerodynamic and surface
255 resistance of evaporation and making the complicated sensible heat calculations are not needed
256 the thing which make this procedure is more simple than others models. The (ϕ) parameter
257 basically depends on and estimated by using LST in a form of rational equation which eliminates
258 the error in LST calculation "if there is error". There are other parameters in eq.5 which entered
259 in calculation of EF such as Δ and γ which depend on air temperature. In this study, we used the
260 air temperature which obtained from the metrological station in order to calculate the Δ and γ ,
261 but there are many studies aimed at correlate the LST and T_{air} in order to dispense of
262 metrological information completely. The second component is the net radiation R_n , which
263 estimated by using eq.8 at daily scale directly rather than instantaneous calculations. ET_a
264 estimated by the proposed procedure validated against actual ET_a adjusted from ET_c by using the
265 $CWSI$ which account for the soil moisture availability. Wheat, potato and sugar beet are three
266 herbaceous crops which were used to test the validity of this procedure. The results showed high
267 agreement and responsible results during different growth stages over these crops. The R^2 values

268 of wheat, potato and sugar beet were 0.88, 0.98 and 0.99 respectively which mean that the
 269 proposed procedure had enough accuracy for wheat, potato and sugar beet at least in our case.

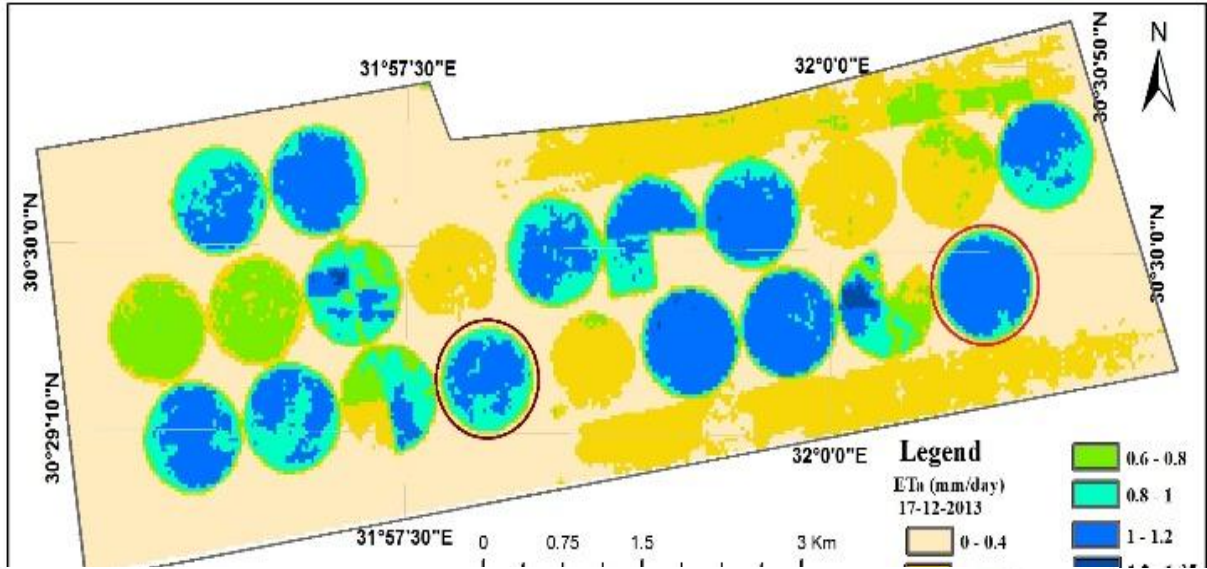


273 (Fig.4) shows matching and the correlation between actual evapotranspiration ETa estimated by
 274 the triangle method and the actual evapotranspiration (ETa_{FPM}) adjusted from FAO-
 275 Penmann-Monteith (FPM) crop evapotranspiration E_{Tc} by using the crop water stress approach
 276 for many crops cultivated in the study area during different growth stages

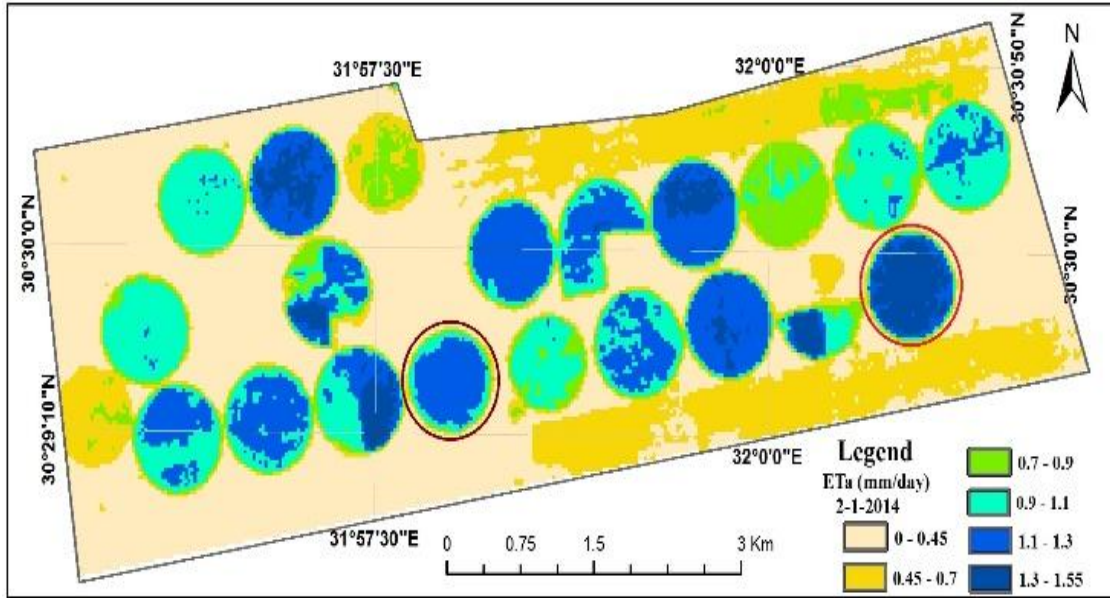
277 Maps of daily ETa were created for all study area crops but for better view, we viewed a part
 278 which contains the studied center pivot units of the different crops in fig.5 and detailed ETa
 279 distribution for these crops (wheat, potato and sugar beet) at different crop stages in fig.6. The
 280 highlighted red, purple and brown circles represent wheat, potato and sugar beet respectively. In
 281 17th of December the ETa values for wheat and sugar beet were 1.1 and 1 mm/day respectively
 282 and the validation values for these crops at the same date were 1.24 and 0.63 mm/day

283 respectively. These values showed good agreement as the wheat and sugar beet where the RMSE
284 were 0.101 and 0.277 respectively. In 2nd of January, the *ETa* values for wheat and sugar beet
285 were 1.35 and 1.17 *mm/day* respectively and the validation values for these crops at the same
286 date were 1.07 and 0.65 *mm/day* respectively. These values showed good agreement as the wheat
287 and sugar beet where the RMSE were 0.201 and 0.37 respectively. In 11th of February, the *ETa*
288 values for wheat, potato and sugar beet were 2.41, 1.2 and 2.25 *mm/day* respectively and the
289 validation values for these crops at the same date were 2.29, 0.86 and 1.9 *mm/day* respectively.
290 These values showed good agreement as the wheat, potato and sugar beet where the RMSE were
291 0.079, 0.23 and 0.24 respectively. In 15th of March, the *ETa* values for wheat, potato and sugar
292 beet were 3.78, 3.1 and 3.16 *mm/day* respectively and the validation values for these crops were
293 3.76, 3.48 and 3.67 *mm/day* respectively. These values showed good agreement as the wheat,
294 potato and sugar beet where the RMSE were 0.013, 0.26 and 0.36 respectively. In 31th of March,
295 the *ETa* values for wheat, potato and sugar beet were 3.87, 3.54 and 3.72 *mm/day* respectively
296 and the validation values for these crops at the same date were 3.75, 3.75 and 4.16 *mm/day*
297 respectively. These values showed good agreement as the wheat, potato and sugar beet where the
298 RMSE were 0.079, 0.15 and 0.31 respectively. In 16th of April, the *ETa* values for wheat, potato
299 and sugar beet were 3.75, 4.3 and 4.66 *mm/day* respectively and the validation values for these
300 crops at the same date were 2.6, 4.4 and 5.14 *mm/day* respectively. These values showed good
301 agreement for potato and sugar beet where the RMSE were 0.06 and 0.32 respectively, but for
302 wheat there was significant error as the RMSE was 0.81. In 2nd of May, the *ETa* values for
303 wheat, potato and sugar beet were 1.3, 1.55 and 4.83 *mm/day* respectively and the validation
304 values for these crops at the same date were 0.8, 1.55 and 5.2 *mm/day* respectively. These values
305 showed good agreement as the wheat, potato and sugar beet where the RMSE were 0.38, 0.004
306 and 0.25 respectively. For crop wheat, there were no significant error at the initial development
307 and mid stages, but at the late stage a high significant error appeared as the RMSE were 0.81 in
308 16th of April and 0.38 in 2nd of May. We interpreted the significant error at the late stage to many
309 reason: 1) at the late stage wheat leaves, especially basal leaves, became almost dead which
310 mean that the cell structure is more weak and able to water absorption than healthy leaves
311 (development and mid stages). 2) sprinkler irrigation system increase the leaves water absorption
312 chance. 3) Continuation of the irrigation process to later stages every day or at least day after
313 day. The previous reasons made the LST and surface albedo (α) down normal, the thing which
314 raise the EF and Rn values respectively. Rising of EF and Rn values led to raising of estimated
315 *ETa* value. Absence of this significant error with potato and sugar beet “ever green until harvest
316 crops” support our interpretation. This mean that the proposed method need to test for wheat
317 under other irrigation systems like surface or drip irrigation.

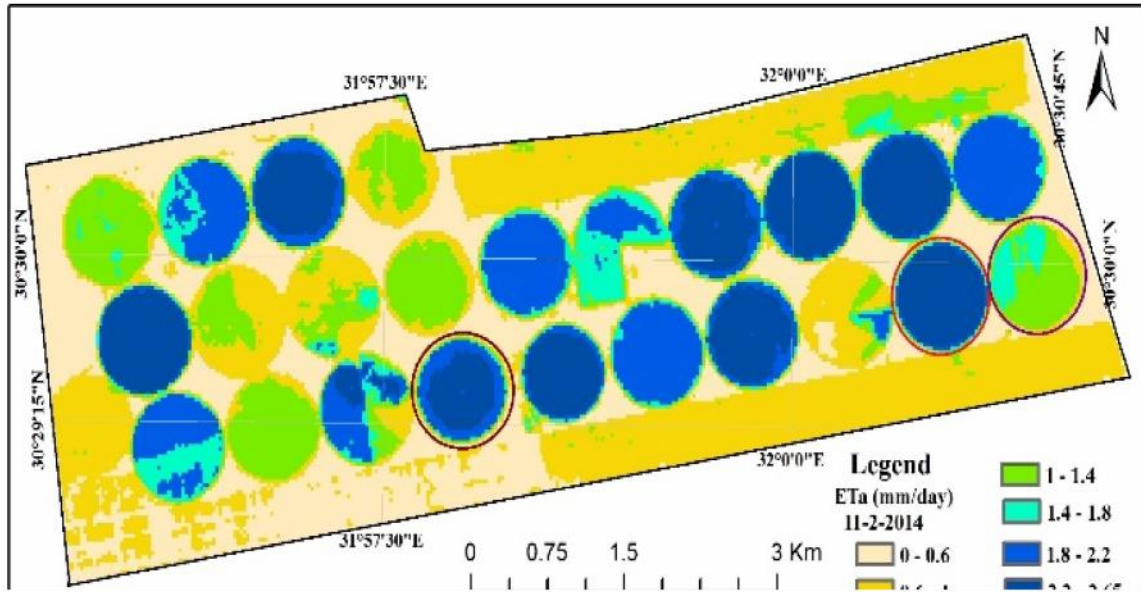
318



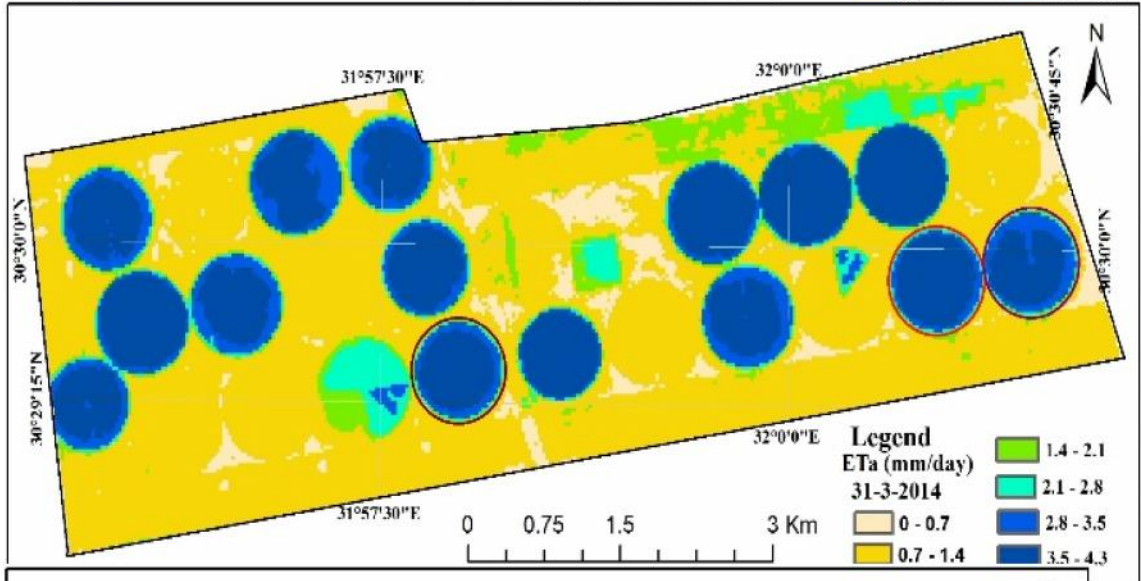
319



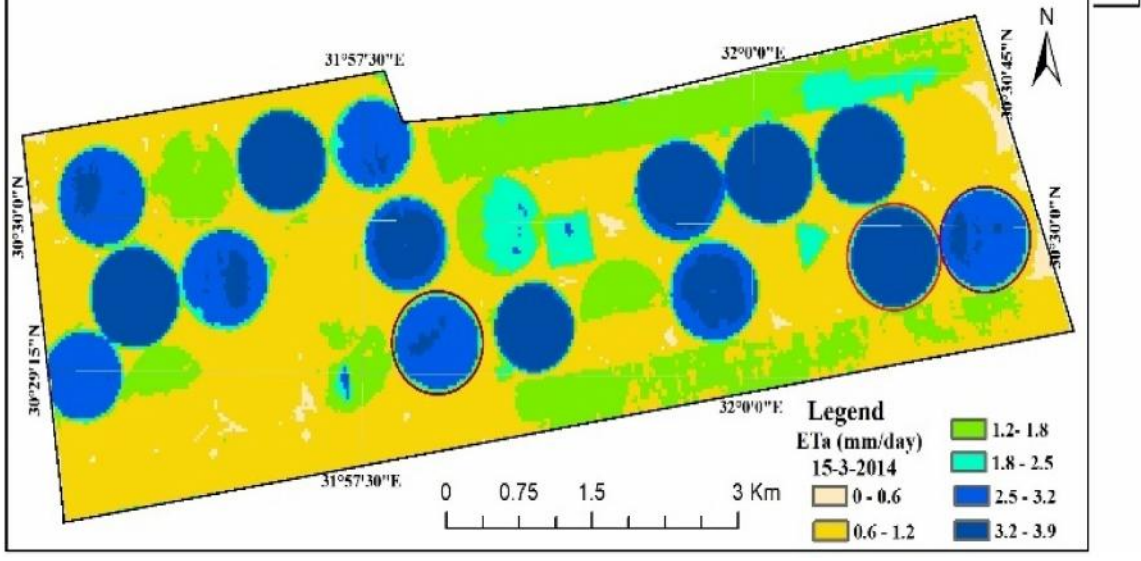
320



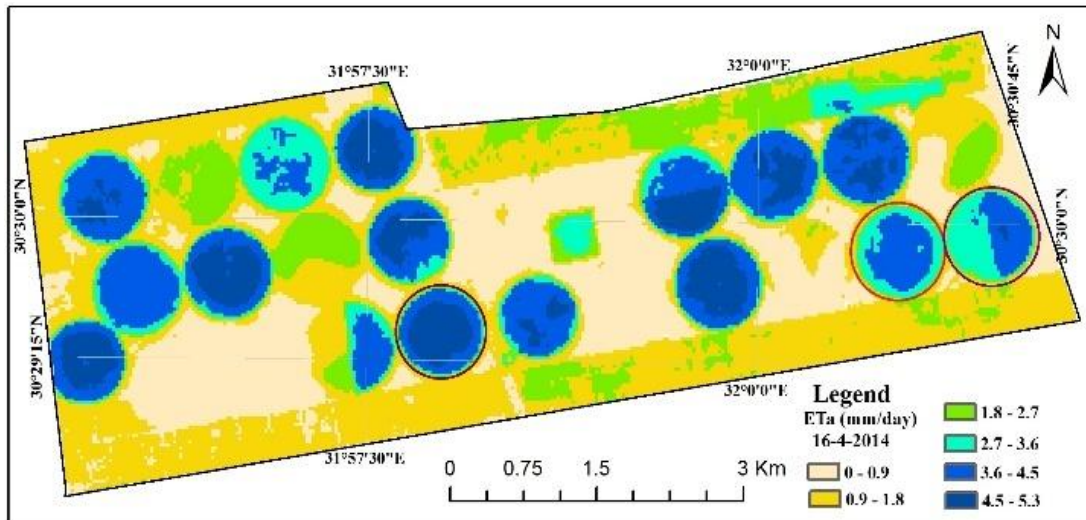
321



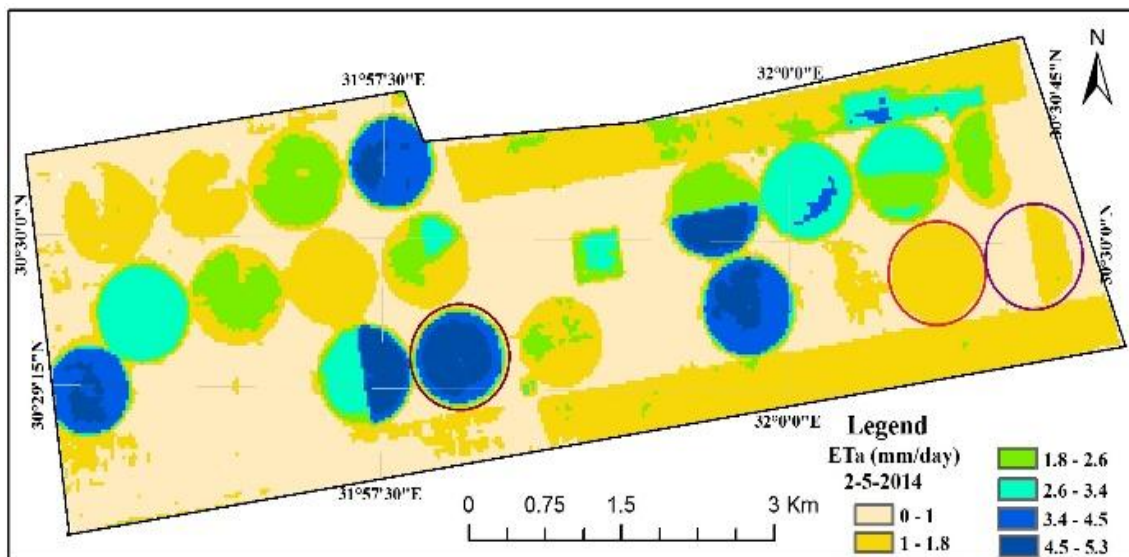
322



323

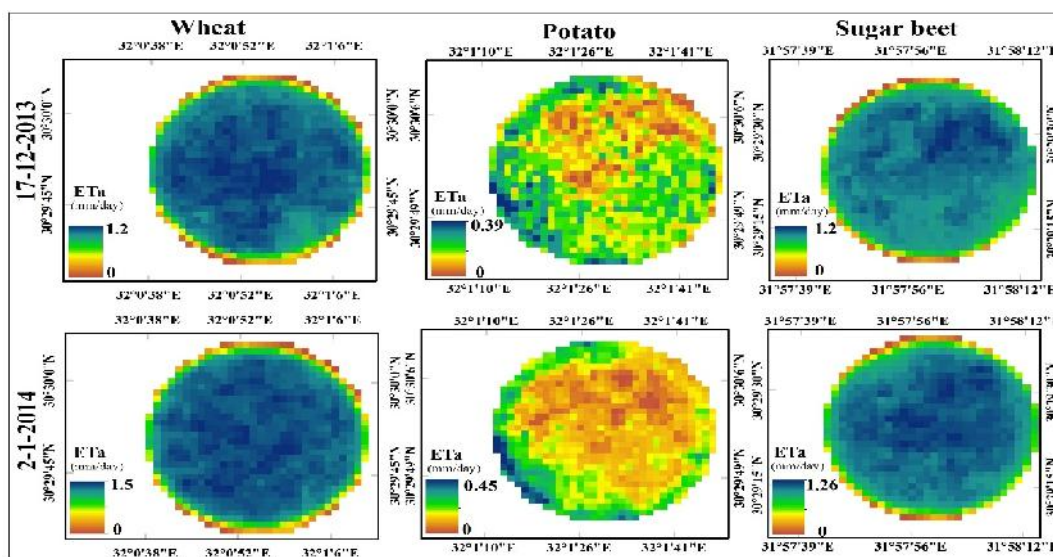


324

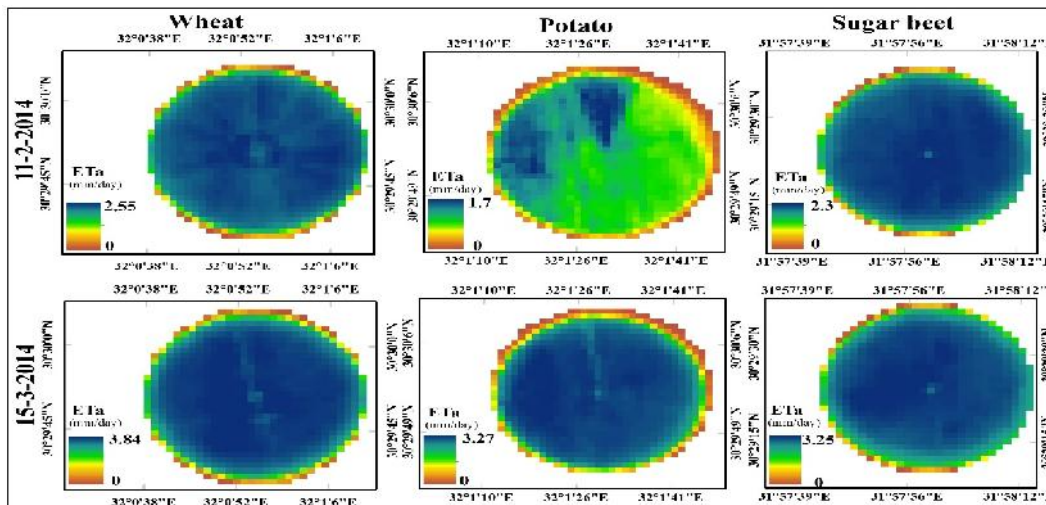


325 (Fig.5) distribution of daily ETa over different crops developing stages during the winter season.

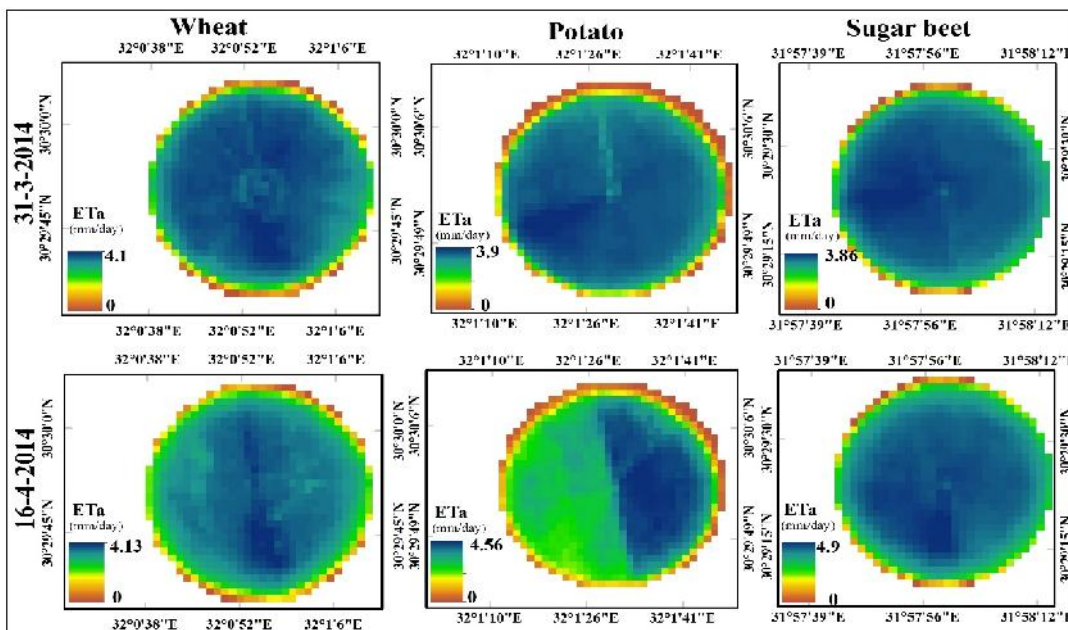
326



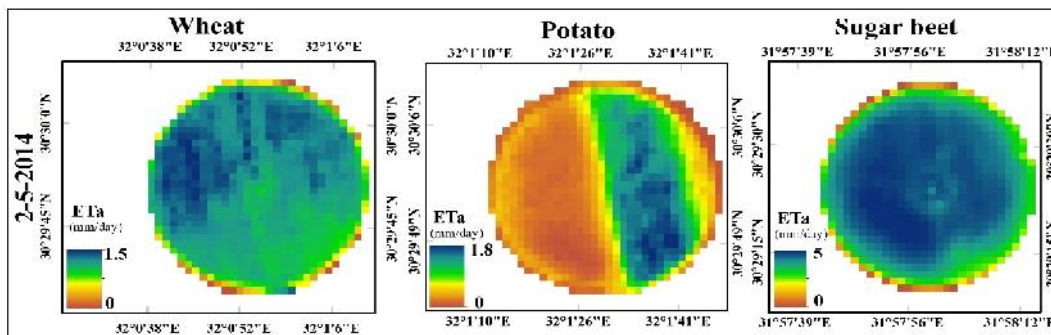
327



328



329



330 (Fig.6) ET_a distribution for wheat, potato and sugar beet crops which used for validation during
 331 different crop stages. (Note: on 17th of December, 2013 and 2nd of January, 2014, the potato
 332 Pivot was not cultivated)

333

334 4. Conclusion

335 Decision-makers and water resources managers are always need to regional information about
336 *ET* to manage water resources distribution. Triangle remote sensing method was proposed by
337 [19-20] and improved by [21]. This method is used for estimating spatial distributed regional *ET*
338 and soil moisture content. Although, this method estimates instantaneous value of Evaporative
339 Fraction (*EF*), it could be used to estimate daily *ET_a* directly; the near noon instantaneous *EF*,
340 which estimated by the triangle method is used as a representative value to the daily average *EF*
341 value which strengthened by the analysis of our climatic data. Actual *ET* at daily scale had been
342 estimated directly for different dates during the winter season over different crops cultivated
343 there. The assessment strategy conducted on three crops, wheat, potato and sugar beet through a
344 comparison between *ET_a* estimated by the proposed procedure and *ET_a* adjusted from *ET_c* using
345 the *CWSI* approach. *ET_c* calculated by using of *ET_o* from FAO Penman-Monteith (FPM)
346 equation and FAO crop coefficient (*K_c*). The *ET_a* values of wheat varied from 1.1 mm/day at
347 the development stage to 3.78 mm/day at the mid stage as the highest value, then 1.3 mm/day at
348 the late stage. Potato graduated from 1.2 mm/day at the initial stage to 4.3 mm/day at the mid
349 stage as the highest value, then 1.55 mm/day at the late stage. The last crop is sugar beet which
350 graduated from 1 mm/day at the initial stage to 4.83 mm/day at the mid stage. The maximum
351 RMSE for the wheat (before the late season), potato and sugar beet is 0.20, 0.26 and 0.37
352 respectively over the different dates. At the late stage of wheat a high significant error appears
353 due to the sprinkler irrigation system effect on the mature wheat. The results showed high
354 agreement between the two methods values during the growing season of the three crops. The *R*²
355 values were 0.88, 0.98 and 0.99 for wheat, potato and sugar beet respectively which mean that,
356 this method is a responsible, realistic and acceptable for estimating daily *ET_a* at regional scale.
357 We recommend that, the proposed method need to evaluate for wheat under other irrigation
358 systems rather than sprinkler irrigation system.

359 5. Reference

- 360 1. Allen RG, Tasumi M, Mores A, Bastiaanssen WGM, Kramber WJ, Anderson H N.
361 [Evapotranspiration from landsat \(SEBAL\): Application in the U.S., proceedings of](#)
362 [Annual Conference of the International Commission on Irrigation and Drainage, Seoul,](#)
363 [Korea. 2001.](#)
- 364 2. Anderson MC, Allen RG, Morse A, Kustas WP. [Use of Landsat thermal imagery in](#)
365 [monitoring evapotranspiration and managing water resources. Remote Sensing of](#)
366 [Environment. 2012; 122: 50-65.](#)
- 367 3. Bastiaanssen WGM. [SEBAL-based sensible and latent heat fluxes in the irrigated Gediz](#)
368 [Basin, Turkey. J Hydrol \(Amst\). 2000; 229:87-100. doi:10.1016/S0022-1694\(99\)00202-](#)
369 [4.](#)
- 370 4. Boegh E, Soegaard H, Thomsen A. [Evaluating evapotranspiration rates and surface](#)
371 [conditions using Landsat TM to estimate atmospheric resistance and surface resistance.](#)
372 [Remote Sens Environ. 2002; 79:329-343. doi:10.1016/S0034-4257\(01\)00283-8.](#)
- 373 5. Boulet G, Chehbouni A, Gentine P, Duchemin B, Ezzahar J, Hadria R. [Monitoring water](#)
374 [stress using time series of observed to unstressed surface temperature difference. Agric](#)
375 [For Meteorol. 2007; 146\(3-4\):159-172.](#)

- 376 6. Caparrini F, Castelli F, Entekhabi D. Estimation of Surface Turbulent Fluxes through
377 Assimilation of Radiometric Surface Temperature Sequences, *J. Hydrometeorol.* 2004; 5:
378 145–159.
- 379 7. Carlson TN, Gillies RR, Schmugge TJ. An interpretation of methodologies for indirect
380 measurement of soil water content. *Agric For Meteorol.* 1995b; 77:191–205.
- 381 8. Crago R D. Conservation and variability of the evaporative fraction during the daytime, *J.*
382 *Hydrol.* 1996; 180:173–194.
- 383 9. De Bruin HAR, Stricker JNM. Evaporation of grass under non-restricted soil moisture
384 conditions. *Hydrol. Sci. J.* 2000;45:391–406.
- 385 10. Droogers P, Immerzeel WW, Lorite IJ. Estimating actual irrigation application by
386 remotely sensed evapotranspiration observations. *Agricultural Water Management.* 2010;
387 97:1351–1359.
- 388 11. Er-Raki S, Chehbouni A, Guemouria N, Duchemin B, Ezzahar J, Hadria R. Combining
389 FAO-56 model and ground-based remote sensing to estimate water consumptions of
390 wheat crops in a semi-arid region. *agricultural water management.* 2007; 87: 41–54.
- 391 12. Galleguillos M, Jacob F, Prévot L, French A, Lagacherie P. Comparison of two
392 temperature differencing methods to estimate daily evapotranspiration over a
393 Mediterranean vineyard watershed from ASTER data, *Remote Sens. Environ.* 2011; 115:
394 1326–1340.
- 395 13. Gillies RT, Carlson TN, Cui J, Kustas WP, Humes KS. A verification of the “triangle”
396 method for obtaining surface soil water content and energy fluxes from remote
397 measurements of the Normalized Difference Vegetation Index (NDVI) and surface
398 radiant temperatures. *Int J Remote Sens.* 1997; 18(15):3145–3166.
- 399 14. Farah H, Bastiaanssen W, Feddes R. Evaluation of the temporal variability of the
400 evaporative fraction in a tropical watershed, *Int. J. Appl. Earth Obs. Geoinf.* 2004; 5:129–
401 140.
- 402 15. Hall F G, Huemmrich K F, Goetz S J, Sellers P J, Nickeson J E. Satellite Remote Sensing
403 of Surface Energy Balance: Success, Failures, and Unresolved Issues in FIFE, *J.*
404 *Geophys. Res.* 1992; 97:19061–19089, doi:10.1029/92jd02189.
- 405 16. Hoedjes J, Chehbouni A, Jacob F, Ezzahar J, Boulet G. Deriving daily evapotranspiration
406 from remotely sensed instantaneous evaporative fraction over olive orchard in semi-arid
407 Morocco, *J. Hydrol.* 2008; 354:53–64.
- 408 17. Jackson RD, Idso SB, Reginato RJ, Pinter PJ. Canopy temperature as a crop water stress
409 indicator. *Water Resour Res.* 1981; 17:1133–1138.
- 410 18. Jia L, Xi G, Liu S, Huang C, Yan Y, Liu G. Regional estimation of daily to annual
411 regional evapotranspiration with MODIS data in the Yellow River Delta wetland, *Hydrol.*
412 *Earth Syst. Sci.* 2009; 13:1775–1787.
- 413 19. Jiang L, Islam S. A methodology for estimation of surface evapotranspiration over large
414 areas using remote sensing observations. *Geophysical Research Letters.* 1999; 26:
415 2773–2776.
- 416 20. Jiang L, Islam S. Estimation of surface evaporation map over southern Great Plains using
417 remote sensing data. *Water Resour Res.* 2001; 37:329–340.
- 418 21. Jiang L, Islam S. An intercomparison of regional latent heat flux estimation using remote
419 sensing data. *International Journal of Remote Sensing.* 2003; 24:2221–2236.

- 420 22. Jiang L, Islam S, Guo W, Jutla A, Senarath S, Ramsay H, Eltahir E. A satellite-based
421 daily actual evapotranspiration estimation algorithm over South Florida. *Global and*
422 *Planetary Change*. 2009; 67:62–77.
- 423 23. Kustas WP, French AN, Hatfield JL, Jackson TJ, Moran MS, Rango A. Remote sensing
424 research in hydrometeorology. *Photogramm Eng Remote Sensing*. 2003a; 69(6):613–646.
- 425 24. Liang S, Rui S, Xiaowen L, Huailiang c, Xuefen Z. Estimating Evapotranspiration Using
426 Improved Fractional Vegetation Cover and Land Surface Temperature Space. *Journal of*
427 *Resources and Ecology*. 2011; 2(3): 225-231.
- 428 25. Li X, Lu L, Yang W, Cheng G. Estimation of evapotranspiration in an arid region by
429 remote sensing—A case study in the middle reaches of the Heihe River Basin.
430 *International Journal of Applied Earth Observation and Geoinformation*. 2012; 17:85–93.
- 431 26. Martha C A, Richard G A, Anthony M, William P K. Use of Landsat thermal imagery in
432 monitoring evapotranspiration and managing water resources. *Remote Sensing of*
433 *Environment*. 2012; 122: 50–65.
- 434 27. Allam MN, Allam GI. Water Resources in Egypt:Future challeges and opportunities.
435 *International Water Resources Association Water International*. 2007; 32 (2):205-218.
- 436 28. Nemani R, Running SW. Estimation of regional surface resistance to evapotranspiration
437 from NDVI and thermal-IR AVHRR data. *J Appl Meteorol*. 1989; 28:276–284.
- 438 29. Norman JM, Kustas WP, Humes KS. A two-source approach for estimating soil and
439 vegetation energy fluxes from observations of directional radiometric surface
440 temperature. *Agric For Meteorol*. 1995; 77:263–293.
- 441 30. Pandey V, Pandey PK, Mahanta AP. Calibration and performance verification of
442 Hargreaves Samani equation in a humid region. *Irrig. Drain*. 2014; 63:659–667.
443 <http://dx.doi.org/10.1002/ird.1874>.
- 444 31. Pankaj KP, Parmendra P. Dabral, Vanita P. Evaluation of reference evapotranspiration
445 methods for the northeastern region of India, *International Soil and Water Conservation*
446 *Research*, <http://dx.doi.org/10.1016/j.iswcr.2016.02.003>
- 447 32. Peng J, Liu Y, Zhao X, Loew A. Estimation of evapotranspiration from MODIS TOA
448 radiances in the Poyang Lake basin, China. *Hydrol. Earth Syst. Sci*. 2013; 17:1431–1444.
- 449 33. Penman HL. Natural evaporation from open water, bare soil and grass, *P. Roy. Soc.*
450 *London Ser. A*. 1948; 193:120–145.
- 451 34. Priestley CHB, Taylor R J. On the assessment of surface heat flux and evaporation using
452 large-scale parameters. *Monthly weather review*. 1972; 100:81–92.
- 453 35. Price JC. Using spatial context in satellite data to infer regional scale evapotranspiration.
454 *IEEE Transactions on Geoscience and Remote Sensing*. 1990; 28:940–948.
- 455 36. Rasmussen MO, Sørensen MK, Wu B, Yan N, Qin H, Sandholt I. Regional-scale
456 estimation of evapotranspiration for the North China Plain using MODIS data and the
457 triangle-approach. *International Journal of Applied Earth Observation and*
458 *Geoinformation*. 2014; 31:143–153.
- 459 37. Roerink GJ, Su Z, Menenti M. S-SEBI: a simple remote sensing algorithm to estimate the
460 surface energy balance. *Phys Chem Earth, Part B Hydrol Oceans Atmos*. 2000;
461 25(2):147–157.
- 462 38. S´anchez JM, Scavone G, Caselles V, Valor E, Copertino VA, Telesca V. Monitoring
463 daily evapotranspiration at a regional scale from Landsat-TM and ETM+ data:
464 Application to the Basilicata region, *J. Hydrol*. 2007; 351:58–70,
465 [doi:10.1016/j.jhydrol.2007.11.041](https://doi.org/10.1016/j.jhydrol.2007.11.041), 2008.

- 466 39. Sandholt I, Ramussen K, Anderson J. A simple interpretation of surface
467 temperature/vegetation index space for assessment of surface moisture status. *Remote*
468 *Sensing of Environment*. 2002; 79:213–224.
- 469 40. Tang R, Li Z, Tang B. An application of the Ts–VI triangle method with enhanced edges
470 determination for evapotranspiration estimation from MODIS data in arid and semi-arid
471 regions: Implementation and validation. *Remote Sensing of Environment*. 2010;
472 114:540–551.
- 473 41. Wang K, Li Z, Cribb M. Estimation of evaporative fraction from a combination of day
474 and night land surface temperatures and NDVI: A new method to determine the
475 Priestley–Taylor parameter. *Remote Sensing of Environment*. 2006; 102:293–305.
- 476 42. Wang KC, Dickinson RE A review of global terrestrial evapotranspiration: Observation,
477 modeling, climatology, and climatic variability. *Reviews of Geophysics*, 50, RG2005.
478 2012; <http://dx.doi.org/10.1029/2011RG000373>.
- 479 43. Yang J, Wang Y. Estimating evapotranspiration fraction by modeling two-dimensional
480 space of NDVI/albedo and day–night land surface temperature difference: A comparative
481 Study. *Advances in Water Resources*. 2011; 34:512–518.
- 482 44. Zwart SJ, Bastiaanssen WGM, Fraiture C, Molden DG. WATPRO: A remote sensing
483 based model for mapping water productivity of wheat. *Agricultural Water Management*.
484 2010; 97: 1628–1636.